Sea surface temperature pattern reconstructions in the Arabian Sea

Kristina A. Dahl[1,2] and Delia W. Oppo[3]

Received 30 March 2005; revised 18 November 2005; accepted 12 December 2005; published 28 March 2006.

[1] Sea surface temperature (SST) and seawater $\delta^{18}O$ ($\delta^{18}O_w$) were reconstructed in a suite of sediment cores from throughout the Arabian Sea for four distinct time intervals (0 ka, 8 ka, 15 ka, and 20 ka) with the aim of understanding the history of the Indian Monsoon and the climate of the Arabian Sea region. This was accomplished through the use of paired Mg/Ca and $\delta^{18}O$ measurements of the planktonic foraminifer *Globigerinoides ruber*. By analyzing basin-wide changes and changes in cross-basinal gradients, we assess both monsoonal and regional-scale climate changes. SST was colder than present for the majority of sites within all three paleotime slices. Furthermore, both the Indian Monsoon and the regional Arabian Sea mean climate have varied substantially over the past 20 kyr. The 20 ka and 15 ka time slices exhibit average negative temperature anomalies of 2.5°–3.5°C attributable, in part, to the influences of glacial atmospheric CO_2 concentrations and large continental ice sheets. The elimination of the cross-basinal SST gradient during these two time slices likely reflects a decrease in summer monsoon and an increase in winter monsoon strength. Changes in $\delta^{18}O_w$ that are smaller than the $\delta^{18}O$ signal due to global ice volume reflect decreased evaporation and increased winter monsoon mixing. SSTs throughout the Arabian Sea were still cooler than present by an average of 1.4°C in the 8 ka time slice. These cool SSTs, along with lower $\delta^{18}O_w$ throughout the basin, are attributed to stronger than modern summer and winter monsoons and increased runoff and precipitation. The results of this study underscore the importance of taking a spatial approach to the reconstruction of processes such as monsoon upwelling.

Citation: Dahl, K. A., and D. W. Oppo (2006), Sea surface temperature pattern reconstructions in the Arabian Sea, *Paleoceanography*, *21*, PA1014, doi:10.1029/2005PA001162.

1. Introduction

[2] Reconstructing the history of the Indian Monsoon is critical for developing an understanding of past, present, and future monsoon variability. Because Arabian Sea sea surface temperatures (SSTs) are sensitive to the strength of Indian Monsoon winds, they can be used to infer monsoon strength through time. During boreal summer, southwest winds associated with the Indian summer monsoon blow over the Arabian Sea (Figure 1). These winds induce coastal upwelling along the Somali and Omani margins. The upwelling is reflected in the SST pattern in the Arabian Sea (Figure 1), which is characterized by a ~4°C temperature gradient increasing from west (24°–25°C) to east (28°C). During the Indian winter monsoon, north-northeast winds from the Asian continent cause mixing and cooling of the surface waters of the northernmost Arabian Sea, north of 20°N. Sites in this region experience a 3°–4°C cooling during this season. On an annually averaged basis, SST in the western Arabian Sea is ~2°C cooler than in the eastern Arabian Sea [*Levitus and Boyer*, 1994].

[3] In addition to being affected by Indian Monsoon winds, Arabian Sea SSTs, like SST everywhere, can be affected by a number of radiative forcing factors, including solar insolation, which varies on seasonal and orbital timescales, greenhouse gas forcing, which includes the concentration of CO_2, and land surface properties, particularly the extent of land ice. The strength of the monsoon itself is, in turn, dependent upon these radiative forcing factors [e.g., *Pinot et al.*, 1999; *Liu et al.*, 2003], although the relative importance of these factors in determining monsoon strength is a subject of debate [*Clemens et al.*, 1991; *Reichart et al.*, 1998; *Clemens and Prell*, 2003]. Nevertheless, climate models forced with either altered solar insolation [*Liu et al.*, 2003] or altered atmospheric CO_2 and land ice [*Pinot et al.*, 1999] show large changes in Arabian Sea SST. Thus Arabian Sea SSTs can vary as a direct response to variations in radiative forcing or indirectly as a response to variations in monsoon strength.

[4] Sea surface salinity (SSS) in the Arabian Sea is relatively high (35–36.5 psu), reflecting high evaporation rates and the input of highly saline waters from the Red Sea and Persian Gulf. Like SST, SSS patterns in the basin vary as a function of season (Figure 1). The waters upwelled during the summer in the western Arabian Sea are marked by relatively low salinities [*Schott et al.*, 2002]. The salinity gradient during the summer monsoon season therefore

[1]Massachusetts Institute of Technology/Woods Hole Oceanographic Institution Joint Program, Woods Hole, Massachusetts, USA.
[2]Now at Scripps Institution of Oceanography, La Jolla, California, USA.
[3]Department of Geology and Geophysics, Woods Hole Oceanographic Institution, Woods Hole, Massachusetts, USA.

0883-8305/06/2005PA001162$12.00

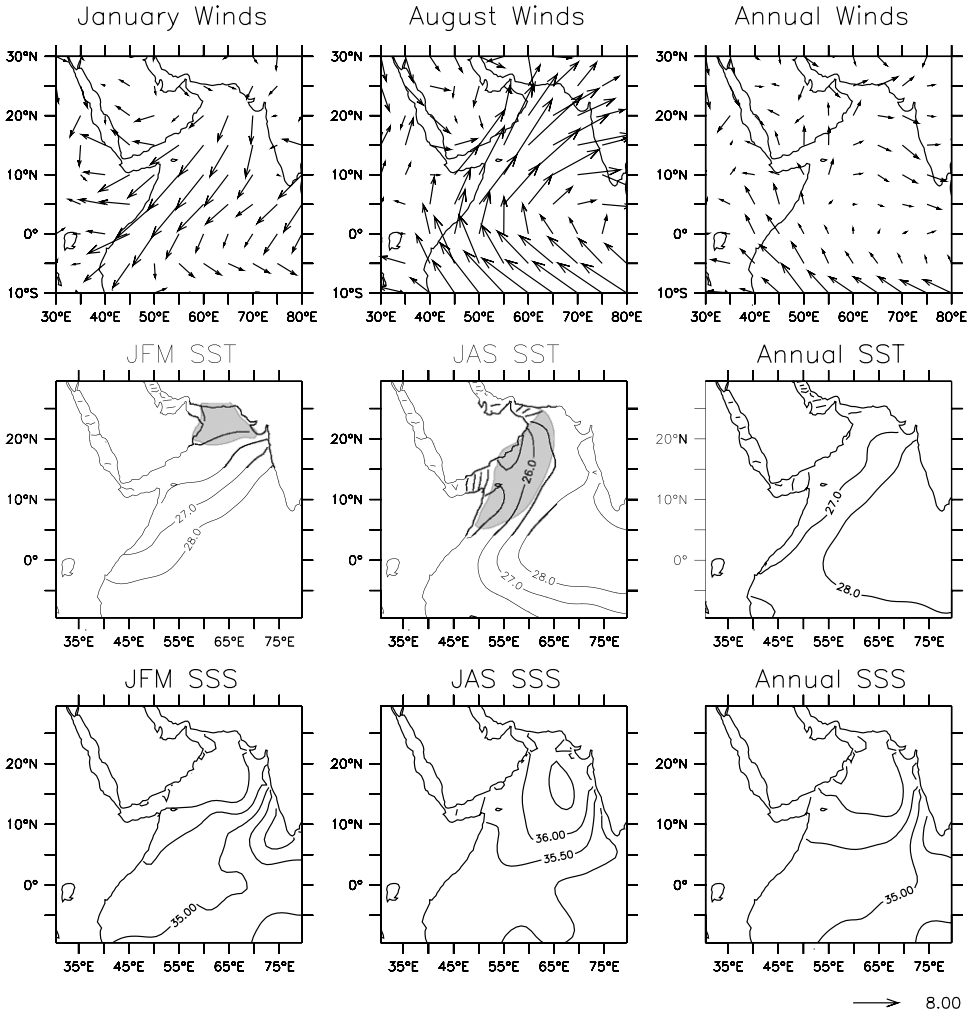

Figure 1. Arabian Sea climatology for winter (left) (January-February-March), summer (middle) (July-August-September), and (right) annual average. Sea surface temperature (SST) and sea surface salinity (SSS) data are from *Levitus and Boyer* [1994]. SSS units are in practical salinity units (psu). Shading indicates regions of winter monsoon mixing and summer monsoon upwelling, respectively. Wind data are provided by the NOAA-CIRES Climate Diagnostic Center, Boulder, Colorado (http://www.cdc.noaa.gov). Units are m s^{-1}.

increases by ~0.5 psu from west to east across the basin. On an annually averaged basis, there is almost no gradient across the basin.

[5] Historically, paleoceanographic time series reconstructions of the Indian Monsoon have taken advantage of signals associated with summer monsoon-induced upwelling in the western Arabian Sea, such as the percentage and/or isotopic composition of specific planktonic foraminifera within the upwelling regions [*Prell*, 1984; *Naidu and Malmgren*, 1995; *Overpeck et al.*, 1996; *Anderson et al.*, 2002; *Gupta et al.*, 2003]. In this study, we reconstruct the Arabian Sea SST pattern for four time periods (0 ka, 8 ka, 15 ka, and 20 ka). By using a suite of sediment cores from throughout the Arabian Sea, we can assess SST changes in both upwelling and nonupwelling regions, thus allowing for discrimination between SST changes induced by local upwelling and regional-scale SST changes that are unlikely to be caused by upwelling. Our SST reconstructions are accomplished using the Mg/Ca ratio of the planktonic foraminifer *Globigerinoides ruber*, which has been shown to be sensitive to SST [e.g., *Anand et al.*, 2003, and references therein]. In addition, by pairing our Mg/Ca SSTs with $\delta^{18}O$ measurements on the same samples, we calculate seawater $\delta^{18}O$ (hereinafter $\delta^{18}O_w$) as a means of reconstructing the surface hydrology of the Arabian Sea.

2. Materials and Methods

[6] The sediment cores used in this study (Figure 2 and Table 1) include box, piston, and gravity cores collected on a number of different cruises. The modern, 8 ka, 15 ka, and 20 ka time horizons were identified previously in each core

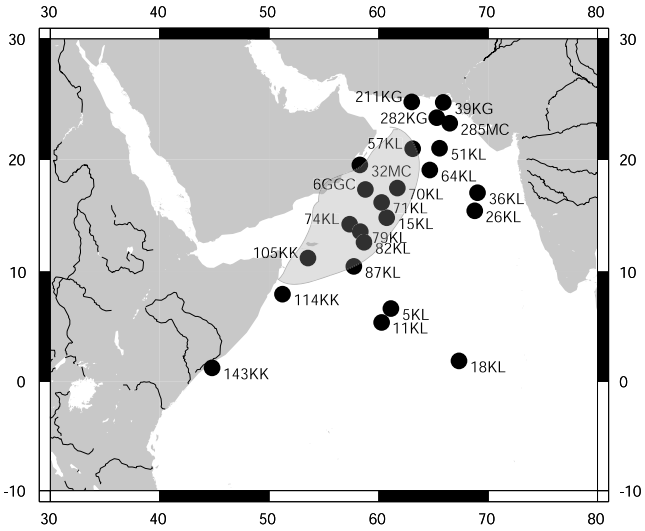

Figure 2. Locations of cores used in this study. Shading indicates the region currently affected by summer monsoon upwelling.

via a combination of oxygen isotope stratigraphies and AMS ^{14}C dates (Table 2 and Figure 3) [*Sirocko*, 1989]. We have recalibrated the ^{14}C dates originally published by *Sirocko* [1989] using Calib 5.0 *Stuiver and Reimer* [1993], which somewhat alters the ages of the time horizons identified by *Sirocko* [1989] and subsequently used in this study. These time slices are primarily intended to be representative of modern, early Holocene, deglacial, and glacial conditions, respectively. While the sedimentation rates and depth ranges for each core and sample indicate that the age range does not exceed 3 kyr for any of the individual samples used in this study, with bioturbation the full age range represented by any given time slice could be somewhat larger. For this reason, the heterogeneities in our SST and $\delta^{18}O_w$ reconstructions are likely due, in large part, to differences in ages of samples within the same time slice. Because these samples were also utilized for several other studies [*Sirocko and Sarnthein*, 1989; *Sirocko et al.*, 1991; *Sirocko and Lange*, 1991; *Sirocko et al.*, 2000], not all of the time slice samples from every core were still available for use. Optimally, we would like carry out a similar study with improved chronologies.

[7] Specimens of *Globigerinoides ruber* (white) were picked from the 212–300 μm size fraction. Each sample, composed of an average of 50 individuals, was then weighed and crushed gently between two glass slides in order to open the individual chambers for effective cleaning. A split of the total sample, representing approximately 10 individuals, was then removed for isotopic analysis, and the remainder was used for Mg/Ca analysis.

[8] Samples for Mg/Ca were ultrasonicated briefly to remove clay particles and then subjected to a series of cleaning treatments designed to remove clays, metal oxides, and organic matter from the shells. Our cleaning procedure followed that of *Boyle and Keigwin* [1985] and subsequent revisions [*Rosenthal et al.*, 1995; *Boyle and Rosenthal*, 1996].

[9] Mg/Ca ratios were measured with a high-resolution sector-field inductively coupled plasma mass spectrometer (ICP-MS) (Finnigan Element2). Mg, Ca, and Al concentrations were determined in low-resolution mode by averaging measurements from 74 scans. All ions were counted in analog mode. Because foraminifera from parts of the Arabian Sea contain stubbornly adhering clays that could

Table 1. Locations of Sediment Samples Used in This Study

Cruise	Core	Time Slices	Latitude	Longitude	Water Depth, m	Sample Depth, cmbsf[a]
SO28	5KL	20	6°39.8′N	61°8.0′E	3335	30–33
SO28	11KL	0, 8, 15, 20	5°23.4′N	60°15.1′E	3859	0–5/11–14/41–44/65–69
SO28	18KL	0, 8, 15, 20	1°54.0′N	67°20.5′E	3035	0–10/17–21/33–37/43–47
SO42	15KL	8, 20	14°52.8′N	64°44.8′E	3920	16–20/50–54
SO42	26KL	0, 8, 15, 20	15°30.9′N	68°45.6′E	3776	0–5/15–19/78–82/103–107
SO42	36KL	0, 8, 15, 20	17°04.5′N	69°02.7′E	2055	0–5/8–12/26–30/43–47
SO42	51KL	8, 15, 20	20°57.9′N	65°33.5′E	2644	28–32/78–82/130–134
SO42	57KL	0, 8, 15, 20	20°54.5′N	63°07.3′E	3422	0–5/28–32/78–82/118–122
SO42	64KL	8, 15, 20	19°4.6′N	64°41.0′E	3281	8–12/58–62/96–100
SO42	70KL	8, 15, 20	17°30.7′N	61°41.8′E	3810	18–22/58–62/82–86
SO42	71KL	8,15	16°14.2′N	60°15.3′E	4029	38–40/70–74
SO42	74KL	0, 8, 15, 20	14°19.3′N	57°20.8′E	3212	9–15/62–66/138–142/200–204
SO42	79KL	8, 15	14°19.3′N	58°19.6′E	4351	38–42/79–83
SO42	82KL	8, 15, 20	12°41.1′N	58°40.6′E	4416	8–10/58–62/100–105
SO42	87KL	0, 15, 20	10°30.1′N	57°44.2′E	3773	0–5/94–98/118–122
SO90	39KG	0	24°50.0′N	65°55.0′E	704	0–2
SO130	211KG	0	24°52.9′N	63°1.6′E	691	0–2
SO130	282KG	0	23°32.3′N	65°19.0′E	988	0–1
SO130	285MC	0	23°5.8′N	66°29.0′E	778	0–1
IOE	105KK	15, 20	11°16.0′N	53°32.5′E	3535	111–119/138–143
IOE	114KK	20	08°00.5′N	51°12.8′E	3843	137–141
IOE	143KK	0, 20	01°15.0′N	44°47.0′E	1522	12–19/253–258
TN47	6GGC	0, 8, 15, 20	17°22.9′N	58°47.7′E	3652	5–6/66–66.5/122–122.5/208–208.5
TN41	32MC	0	19°30.1′N	58°28.1′E	784	0–1

[a]Centimeters below seafloor.

Table 2. Previously Unreported ^{14}C Dates

Cruise	Core	Depth, cmbsf [a]	Method	Foraminifer Species	^{14}C Age, years	SD,[b] years	Calendar Age, years[c]
TN-47	6GGC	5–6	AMS	mixed planktonics	755	35	270
TN-47	6GGC	37–38	AMS	mixed planktonics	1,730	40	1,090
TN-47	6GGC	80–81	AMS	*G. ruber*, *G. sacculifer*[d]	10,000	70	10,660
TN-47	6GGC	130–131	AMS	*G. ruber*	13,950	80	15,830
TN-47	6GGC	203–204	AMS	mixed planktonics	18,000	90	20,520
TN-47	6GGC	219–219.5	AMS	mixed planktonics	19,100	140	22,090

[a]Centimeters below seafloor.
[b]SD, standard deviation.
[c]Calibrated with a reservoir age of 600 years using Calib 5.0 [*Stuiver and Reimer*, 1993].
[d]Without sac-like final chamber.

potentially elevate the measured Mg/Ca [*Bice et al.*, 2005], we also monitored Al/Ca ratios. Samples with Al/Ca values greater than 30 μmol mol^{-1}, twice that observed in foraminifera considered to have no detrital clay contamination, were excluded from the final data set (three samples total) [*Lea et al.*, 2003; *Schmidt et al.*, 2004]. A standard, containing high-purity elements in ratios consistent with those observed in foraminifera, and a blank of 2% HNO_3 were run between every four samples. The instrumental error for Mg/Ca, calculated from repeated measurements of a series of consistency standards, is 0.03 μmol mol^{-1}.

[10] In order to convert measured Mg/Ca ratios to SST, we used the calibration of *Rosenthal and Lohmann* [2002]. This calibration incorporates shell weight in order to correct for dissolution, which preferentially removes Mg from the foraminiferal tests. This calibration accounts for the fact that our samples, which come from a wide range of depths within the Arabian Sea, likely experience differing degrees of dissolution. The combined instrumental and calibrative errors associated with our calculated Mg/Ca SST is estimated to be ±1°C.

[11] Stable isotopes were measured using a Finnigan MAT 253 coupled to a Kiel III carbonate device. The analytical precision of this instrument for $\delta^{18}O$, as determined by replicate analyses (n = 600) of the carbonate standard NBS19 is 0.07‰. $\delta^{18}O_w$ was calculated using the *G. ruber*–specific calibration of *Mulitza et al.* [2003]: $\delta^{18}O_{w,VSMOW} = (T_{Mg/Ca} - 14.2)/4.44 + \delta^{18}O_{carbonate,VPDB} + 0.27$.

[12] At sites for which we had both a modern and a time slice measurement of Mg/Ca SST and $\delta^{18}O_w$, time slice SST and $\delta^{18}O_w$ anomalies were calculated using the values from the same core. For several sites, however, we had time slice samples without a modern sample from the same core. In these instances, SST anomalies were calculated using the time slice sample and the nearest available core top value. Anomalies calculated by the latter method are denoted in all the figures by open circles as opposed to solid circles.

3. Results and Discussion

3.1. Time Slice: 0 ka

3.1.1. SST

[13] With the exception of three data points, the Mg/Ca-derived SSTs for each site comprising the 0 ka time slice fall within the modern observed SST range at that site (Figures 4 and 5 and Table 3) [*Levitus and Boyer*, 1994]. At most sites, Mg/Ca SSTs are either at or slightly below the observed annual average SST, in accordance with the observation that *G. ruber* lives year round in the Arabian Sea, but experiences blooms during both monsoon seasons and calcifies above 80 m water depth [*Curry et al.*, 1992; *Conan and Brummer*, 2000; *Peeters et al.*, 2002]. The reconstructed west-to-east SST gradient of 2°–4°C is consistent with the observed annually averaged and summer SST gradients of 2°C and 4°C, respectively. As is evident from Figure 5, coverage for the eastern Arabian Sea is not as complete as for the western Arabian Sea. While a greater number of cores for the eastern Arabian Sea would be desirable, it is encouraging that the two sites in the eastern Arabian Sea yield estimates of modern SST that are consistent with one another and with observations.

3.1.2. The $\delta^{18}O_w$

[14] The core top data show a west-to-east gradient in $\delta^{18}O_w$ of 0.3‰, with the west being lower than the east (Figure 5). The relationship between $\delta^{18}O_w$ and salinity in the Arabian Sea varies from location to location and depends heavily upon the abundance of Red Sea waters (Figure 6). The salinity-$\delta^{18}O_w$ relationship observed by *Delaygue et al.* [2001] (crosses in Figure 6), for example, is different from that observed during the JGOFS study (circles in Figure 6; see Table 4; W. Curry, unpublished data, 1995). The *Delaygue et al.* [2001] data are heavily concentrated in the Red Sea and Gulf of Aden regions, and therefore reflect the properties of these local water masses. In contrast, the JGOFS data set includes samples from the western, central, and eastern Arabian Sea. It is therefore difficult to define a single basin-wide salinity-$\delta^{18}O_w$ relationship for the entire Arabian Sea.

[15] Surface seawater $\delta^{18}O$ at a given location is determined by elements of the local hydrological cycle, including precipitation, evaporation, runoff, and advection of water from other locations. The Arabian Sea is an evaporative basin [*Oberhuber*, 1988], which results in heavy surface $\delta^{18}O_w$ values and lower subsurface $\delta^{18}O_w$ values. The modern $\delta^{18}O_w$ and observed salinity gradients across the Arabian Sea are the product of two phenomena: (1) Upwelling in the western Arabian Sea associated with the summer monsoon brings fresher water to the surface, and (2) the western Arabian Sea experiences greater convection and precipitation than the eastern Arabian Sea.

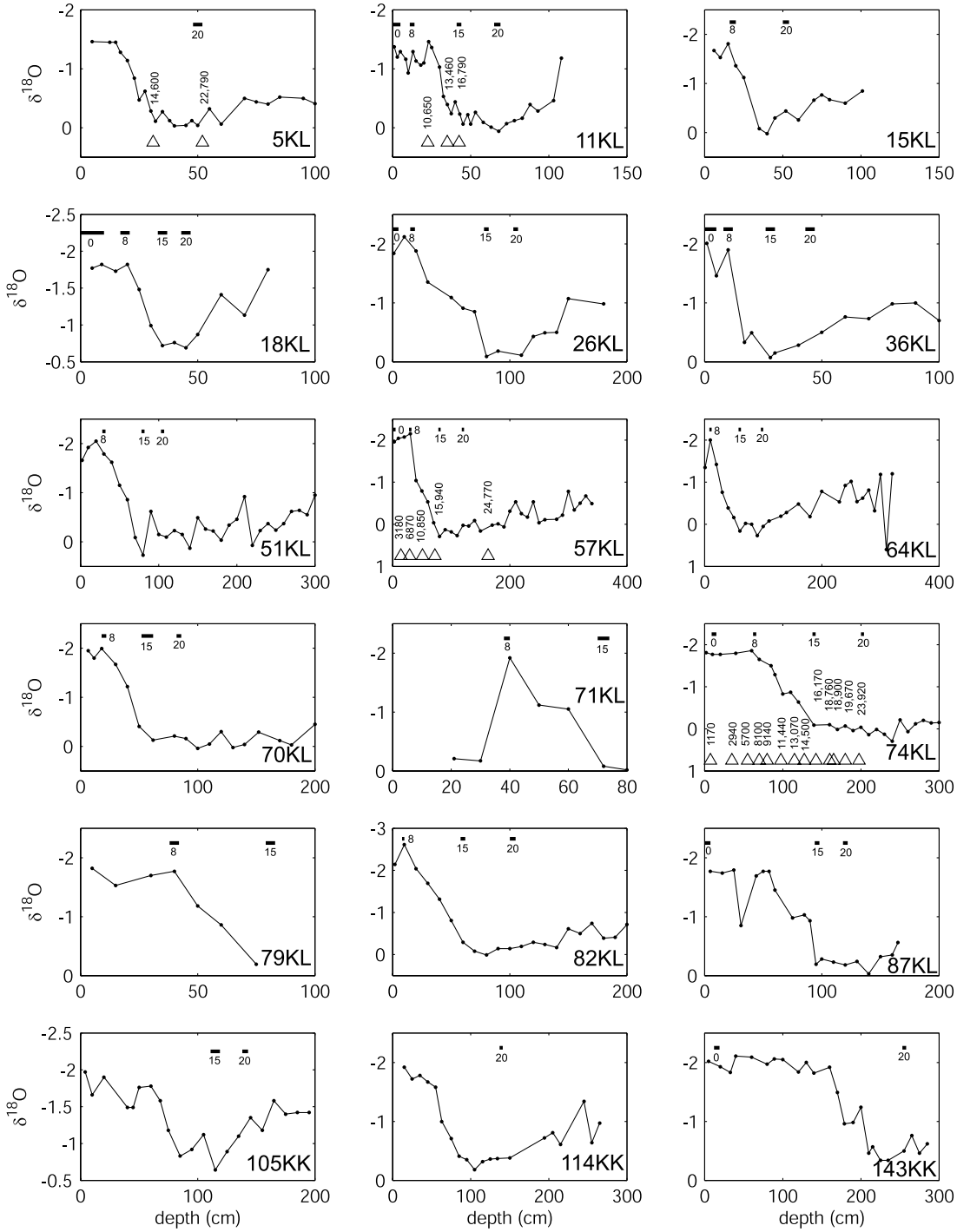

Figure 3. Oxygen isotope and ^{14}C chronologies for cores used for nonmodern time points (with the exception of 6GGC). Data were originally published by *Sirocko* [1989] with ^{14}C dates recalibrated for this study using Calib 5.0 [*Stuiver and Reimer*, 1993]. Triangles indicate ^{14}C dates. Horizontal bars indicate the depth range encompassed by each time slice sample used for this study. For more information regarding the sampling protocol, please see *Sirocko* [1989].

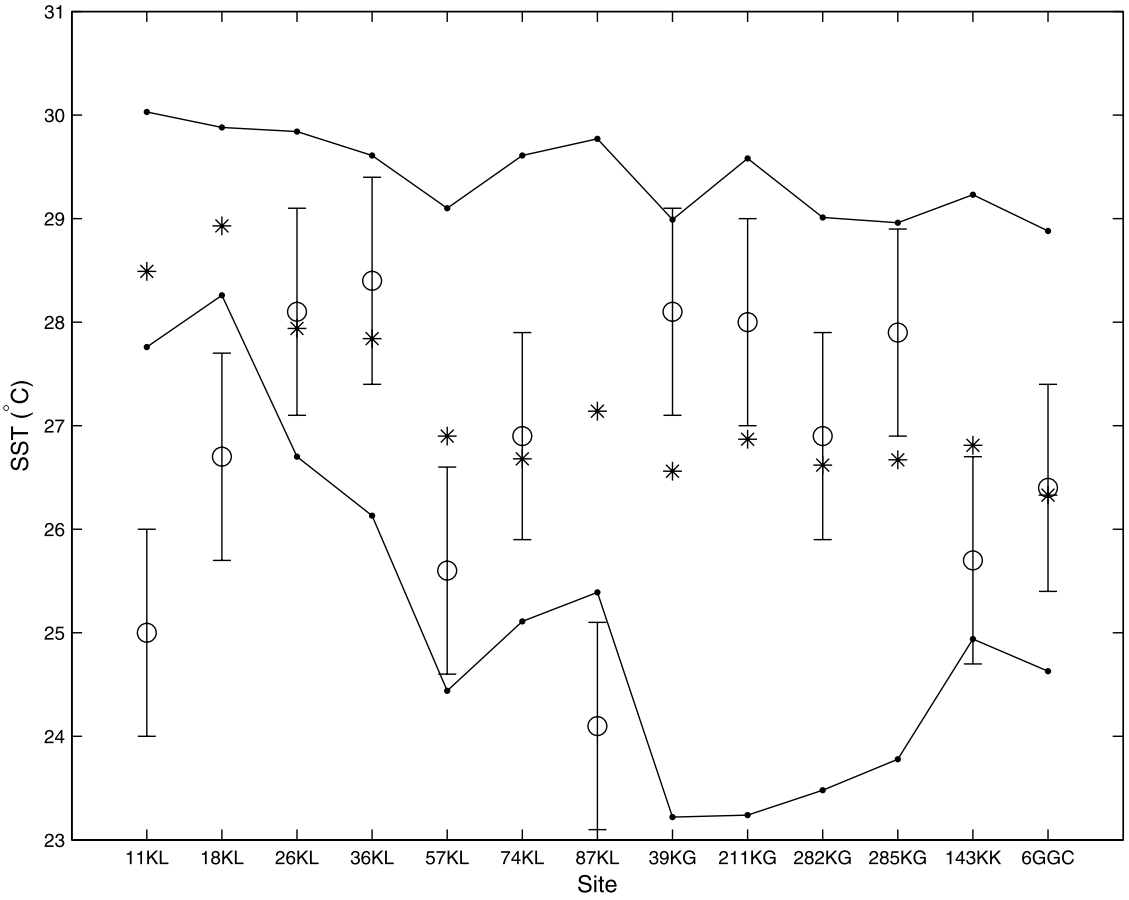

Figure 4. Mg/Ca SST derived from core tops throughout the Arabian Sea (open circles) compared to the maximum and minimum SSTs experienced at each site (lines) and the annual average observed SST (asterisks). Observational data are from *Levitus and Boyer* [1994].

Both of these processes serve to depress salinity and $\delta^{18}O_w$ in the western Arabian Sea relative to the eastern Arabian Sea.

[16] Our core top data are consistent with modern observations of lower salinities in the western than in the eastern Arabian Sea during the summer upwelling season [*Levitus and Boyer*, 1994]. In terms of absolute value, our modern $\delta^{18}O_w$ data are higher than observations by up to 1‰ (G. A. Schmidt et al., Global seawater oxygen-18 database, available at http://data.giss.nasa.gov/o18data, 1999). This discrepancy is likely due to a combination of sources of error including those associated with the calcification depth of, and therefore the temperature recorded by, the foraminifera, and the calibrations for the Mg/Ca-SST relationship and the SST-$\delta^{18}O_w$-$\delta^{18}O_c$ relationship. These errors are presumably temporally invariant; thus, while they affect the absolute values of the calculated $\delta^{18}O_w$, they do not affect the anomalies upon which we focus in subsequent sections.

3.2. Time Slice: 20 ka

[17] The 20 ka time slice lies within the last glacial period, just after the Last Glacial Maximum (LGM; 21 ka) [e.g., *Mix et al.*, 2001]. Given both the temporal proximity of this time slice to the LGM and the uncertainty in our age models for many of the cores used in this study, we will hereinafter refer to this time slice as an LGM time slice. At this time, solar insolation was within 1 W m^{-2} of present-day values (Figure 7) [*Berger and Loutre*, 1991]. However, glacial atmospheric CO_2 concentrations [*Monnin et al.*, 2001] and greater ice volume, combined, were responsible for a ~4 W m^{-2} decrease in global net radiative forcing relative to today [*Broccoli*, 2000].

3.2.1. SST

[18] At the LGM, SST throughout the Arabian Sea was colder than it is today (Figure 8). Colder than present SSTs are evident at sites today affected by monsoon upwelling and mixing (shaded regions) as well as those that are not affected by such processes (unshaded regions). The average SST anomaly relative to present was -3.6 ± 1.8°C (1σ error bars). Such a response is consistent with a climate model simulation of the LGM using an atmospheric–mixed layer ocean model [*Broccoli*, 2000]. Because there was no simulation of upwelling or other oceanic processes within this model, the 2°C Arabian Sea cooling predicted by the model resulted from atmo-

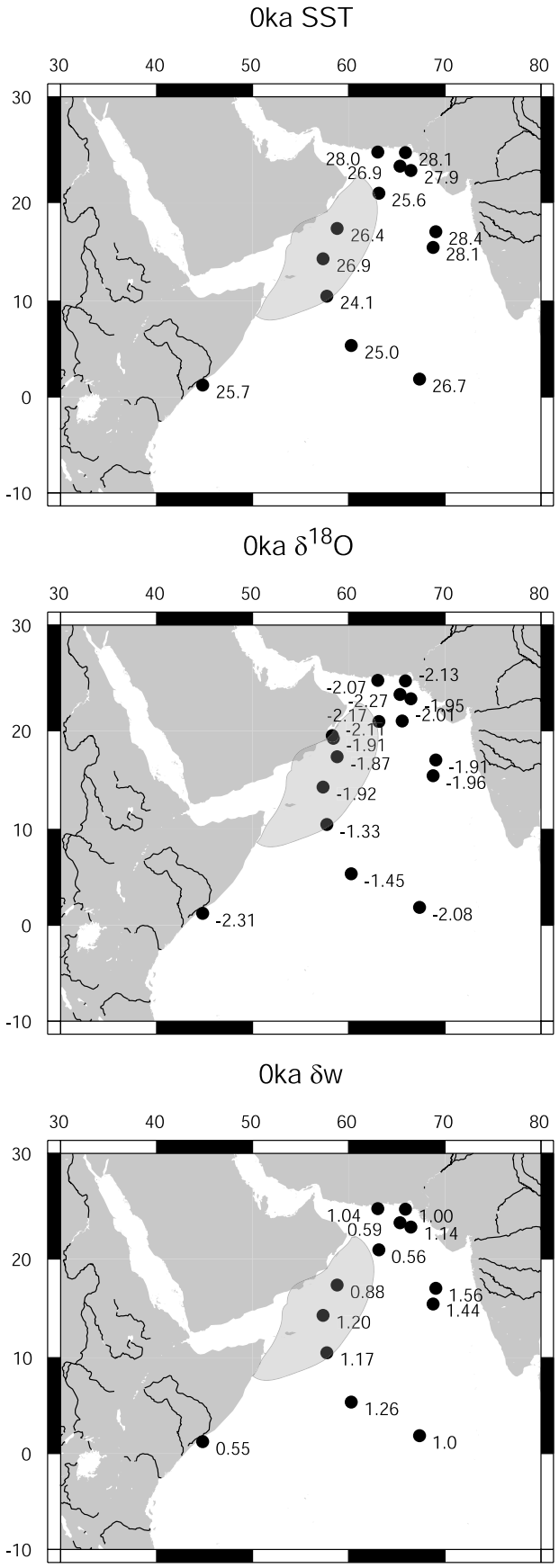

spheric-only mechanisms, namely a prescribed lowering of CO_2 and changes in continental ice that result in changes in atmospheric circulation and, in turn, wind strength and evaporative cooling. The basin-wide cold SST anomalies as determined via our data suggest that the Arabian Sea, like much of the rest of the tropics, could have cooled as a direct result of decreased radiative forcing. It is also important to note, however, that the disappearance of the west-to-east SST gradient within this time slice implies that the strength of Indian Monsoon was altered during this time. The lack of a gradient results from larger cold anomalies in the eastern Arabian Sea than in the western Arabian Sea. This SST pattern could result from a weakened summer monsoon (and therefore decreased upwelling and a subsequent relative warming) either on its own or in conjunction with a strengthened winter monsoon (and therefore enhanced mixing and cooling of surface waters in the northern and eastern Arabian Sea). Either scenario is consistent with both climate model simulations of the LGM [*Pinot et al.*, 1999] and our understanding of the response of the monsoon to changes in solar activity derived from modern data [*Kodera*, 2004]. Paleoclimate data, climate models, and instrumental data all suggest that the summer monsoon is weak during times of low solar heating [e.g., *Fontugne and Duplessy*, 1986; *Pinot et al.*, 1999; *Sirocko et al.*, 2000; *Kodera*, 2004].

3.2.2. LGM Comparison With Alkenone and Transfer Function Data

[19] On the basis of foraminiferal transfer function reconstructions of SST, the CLIMAP study concluded that LGM SSTs in the Arabian Sea were within 1°C of present-day SSTs [*CLIMAP Project Members*, 1981]. Since then, a number of investigations employing the use of alkenones [*Rostek et al.*, 1993; *Emeis et al.*, 1995; *Bard et al.*, 1997; *Rostek et al.*, 1997; *Sonzogni et al.*, 1998; *Higginson et al.*, 2004] and foraminiferal abundances [*Cayre and Bard*, 1999; *Naidu and Malmgren*, 2005] have suggested that LGM SSTs were in fact on the order of 3°C cooler than present. With the exception of *Sonzogni et al.* [1998], these studies have utilized a time series approach, thus giving a temporal, rather than spatial, history of SST. As noted by *Sonzogni et al.* [1998], alkenone-derived SSTs are systematically lower than estimates derived from transfer functions and/or the modern analog technique at the same site. Mg/Ca and alkenone data from nearby cores suggest that Mg/Ca-derived SSTs may be still lower than alkenone SSTs, although both proxies suggest a basin-wide negative SST anomaly of ~2–4°C for the LGM. Unlike our Mg/Ca data, the spatially distributed alkenone data of *Sonzogni et al.* [1998] show a similar magnitude of cold anomalies in both the eastern and western parts of the Arabian Sea. Offsets between alkenone and Mg/Ca SST estimates may result from differences in the seasonality of the production of alkenone-producing coccoliths and foraminifera. Nonetheless, the Mg/Ca data presented here

Figure 5. Surface conditions reconstructed from core top (0 ka) sediments: (top) Mg/Ca SST, (middle) $\delta^{18}O$, and (bottom) $\delta^{18}O_w$. Shading is as for Figure 2.

Table 3. Raw Shell Weight and Mg/Ca Data

Core	Time, ka	Average Shell Weight, μg	Mg/Ca, mmol mol^{-1}	SST
11KL	0	8.97	3.60	25.0
18KL	0	8.83	4.20	26.7
26KL	0	8.59	4.70	28.1
36KL	0	10.14	5.40	28.4
57KL	0	8.25	3.61	25.6
74KL	0	7.66	3.90	26.9
87KL	0	10.17	3.60	24.1
39KG	0	8.48	4.65	28.1
211KG	0	8.56	4.63	28.0
282KG	0	9.38	4.46	26.9
285MC	0	8.72	4.64	27.9
143KK	0	11.32	4.50	25.7
06GGC	0	6.13	5.70	26.4
11KL	8	10.76	3.69	23.9
15KL	8	12.58	3.82	23.1
18KL	8	9.80	4.06	25.6
26KL	8	12.77	4.71	25.2
36KL	8	12.21	4.29	24.6
51KL	8	9.63	3.63	24.6
64KL	8	8.68	3.85	25.9
70KL	8	10.85	3.80	24.2
71KL	8	9.85	3.91	25.2
74KL	8	8.93	4.10	26.4
79KL	8	9.26	3.76	25.2
82KL	8	9.00	4.22	26.7
87KL	8	10.00	3.89	25.1
06GGC	8	9.30	3.62	24.8
11KL	15	10.61	3.26	22.7
18KL	15	12.03	3.01	21.0
26KL	15	14.76	3.57	21.1
36KL	15	12.84	4.18	23.9
51KL	15	12.20	4.98	26.2
57KL	15	12.11	4.49	25.1
64KL	15	11.92	3.99	24.0
70KL	15	9.11	3.37	24.2
71KL	15	11.55	4.88	26.4
74KL	15	10.72	4.06	25.0
79KL	15	10.00	3.087	22.6
82KL	15	8.94	3.53	24.8
87KL	15	11.40	3.17	21.9
105KK	15	9.67	4.017	25.6
06GGC	15	9.70	2.80	21.8
5KL	20	11.00	3.05	21.8
11KL	20	9.15	3.32	24.0
15KL	20	9.55	3.32	23.7
18KL	20	10.74	3.28	22.7
26KL	20	11.00	2.76	20.7
36KL	20	10.59	3.69	24.1
51KL	20	11.86	3.11	21.4
64KL	20	10.17	3.21	22.9
70KL	20	8.79	3.63	25.3
74KL	20	10.40	3.02	22.1
82KL	20	9.78	3.09	22.8
87KL	20	10.10	3.00	22.2
105KK	20	8.66	3.76	25.7
114KK	20	10.89	3.12	22.1
143KK	20	9.89	3.27	23.3
06GGC	20	8.50	2.86	23.0

provides further evidence for a greater cooling in the Arabian Sea than had been originally suggested by CLIMAP.

3.2.3. The $\delta^{18}O_w$

[20] Globally, $\delta^{18}O_w$ was approximately 1‰ higher at the LGM than it is today [*Fairbanks*, 1989; *Schrag et al.*, 2002, and references therein]. Although $\delta^{18}O_w$ at most sites in the Arabian Sea was higher than present at the LGM, the increase at most sites was considerably less than 1‰ (Figure 8). Sites within the western Arabian Sea experienced increases of 0.4–0.7‰ while sites in the eastern Arabian Sea experienced almost no change in $\delta^{18}O_w$ relative to today. These results suggest a reversal of the $\delta^{18}O_w$ gradient observed in our 0 ka samples such that, during the LGM, the eastern Arabian Sea was characterized by lower values than the western Arabian Sea.

[21] The dampened increase in $\delta^{18}O_w$ relative to the global mean could be the result of a number of factors. Given the cool SSTs in the Arabian Sea at this time, evaporation was likely lower. Today, evaporation results in a positive $\delta^{18}O_w$ gradient of 0.1–0.3‰ from the surface to 100 m depth. A decrease in evaporation would therefore decrease surface $\delta^{18}O_w$ values. Such a decrease could partially offset the global increase in $\delta^{18}O_w$. The reversal of the modern gradient implies that changes in the strength of the summer and winter monsoons could also be affecting $\delta^{18}O_w$ values. More specifically, weaker (stronger) than present summer (winter) monsoon upwelling (mixing) could be responsible for the fact that the positive western Arabian Sea $\delta^{18}O_w$ anomaly increase was significantly larger than that of the eastern Arabian Sea. It is also possible that the decrease in the outflow of highly saline waters from the Red Sea through the shallow (137 m) Strait of Bab-el-Mandeb, proposed by *Locke and Thunell* [1988] and *Naqvi and Fairbanks* [1996], caused a relative freshening of Arabian Sea waters.

3.3. Time Slice: 15 ka

[22] Insolation conditions at 30°N at 15 ka were markedly different from those at 20 ka (Figure 7). Between 20 ka and 15 ka, annually averaged insolation increased by 6 W m^{-2} [*Berger*, 1978]. However, global ice volume was still higher than at present [*Fairbanks*, 1989; *Bard et al.*, 1996], and CO_2 was still at near-glacial values (200 ppmv) [*Monnin et al.*, 2001].

3.3.1. SST

[23] All sites included in this study had cooler SSTs at 15 ka than they do today (Figure 9). The average negative temperature anomaly for this time slice is 2.9° ± 2.2°C. The greatest anomalies occur at sites that lie outside of the modern summer upwelling region. That this time slice is generally cold in our study is consistent with the fact that temperatures in the North Atlantic at 15 ka were colder than during the LGM [*Waelbroeck et al.*, 1998; *Bard et al.*, 2000]. This cold period in the North Atlantic is known as Heinrich event 1 (H1). The chronology for our cores is not sufficient enough to state for certain that we have captured H1. However, it seems likely given the cold SSTs observed within this time slice. That SST remained cold at this time despite greatly increased solar insolation suggests that the influence of glacial boundary conditions outweighed the influence of solar insolation. If, in fact, this time slice does capture H1, the data are consistent with the hypothesis that the Asian monsoon system is subject to downstream effects from the North Atlantic region [*Kutzbach et al.*, 1993].

[24] Again, insight into the impact of the Indian Monsoon on SST during this time can be gained by evaluating the SST gradient across the Arabian Sea. SST anomalies for the

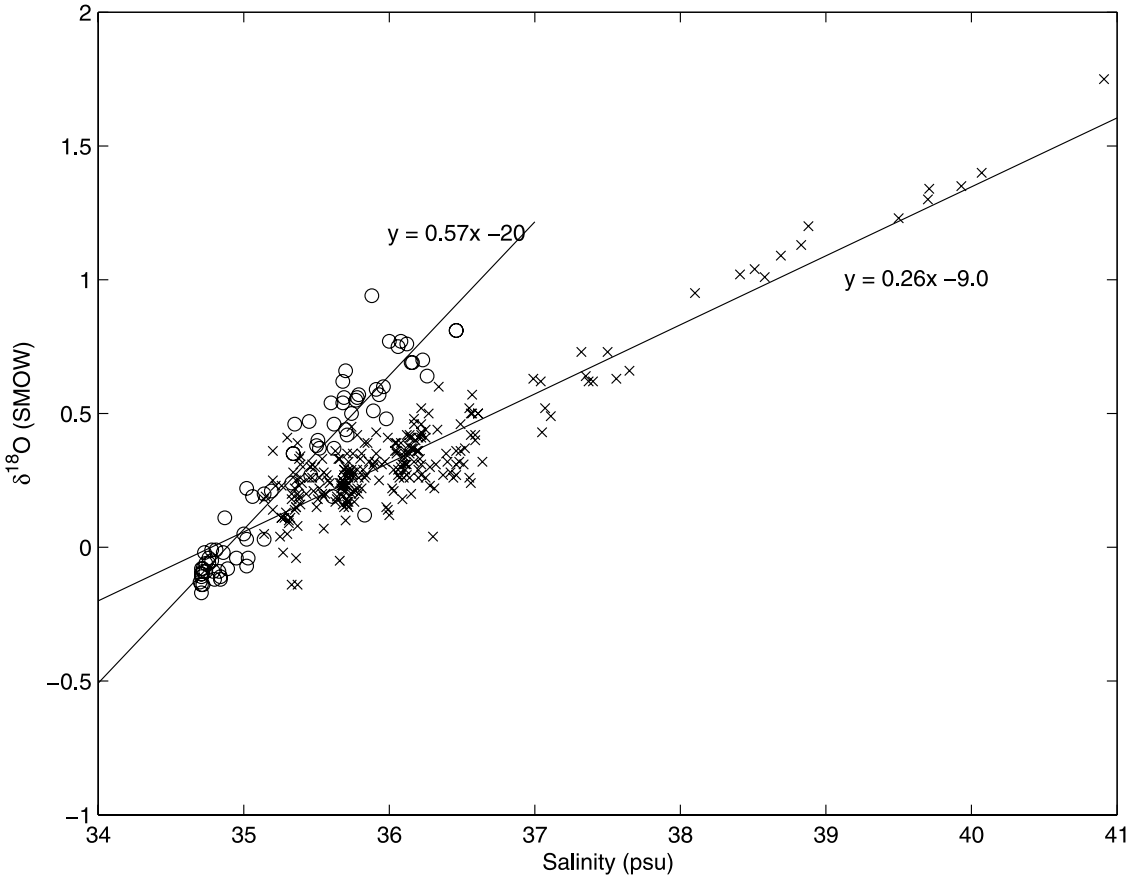

Figure 6. Salinity-$\delta^{18}O_w$ relationships for the Arabian Sea. Crosses denote surface data from *Delaygue et al.* [2001] ($r^2 = 0.85$ and $r = 0.92$). This data set is heavily sampled in the Gulf of Aden region and likely reflects the large influence of Red Sea water. Circles denote full water column data from this study obtained during Joint Global Ocean Flux Study cruises TN-041 and TN-047 (1994 and 1995, respectively; $r^2 = 0.90$ and $r = 0.95$). This data set includes stations in the western, central, and eastern Arabian Sea. Note that the two data sets overlap significantly but that the slopes defining the salinity-$\delta^{18}O_w$ relationships differ.

western Arabian Sea sites are heterogeneous, ranging from −0.5°C to −4.3°C. Given this heterogeneity, it appears that the west-to-east SST gradient was either nonexistent or reversed during this time. This implies an increase in the strength of the winter monsoon (and a greater cooling of SST in the northeastern Arabian Sea via mixing) and a decrease in the strength of the summer monsoon (and a relative warming of western Arabian Sea SSTs via reduced upwelling) relative to today.

3.3.2. The $\delta^{18}O_w$

[25] At 15 ka, $\delta^{18}O_w$ in the Arabian Sea was higher than it is today by an average of 0.73‰ (Figure 9). This positive anomaly is close to that of the global mean of 0.75‰ [*Fairbanks*, 1989], which implies that ice volume changes are largely responsible for the higher conditions exhibited in this time slice. While the data, like the SST data for this time slice, are heterogeneous, the average positive anomaly in the west is greater than that in the east by 0.3‰. Thus, as was the case for the 20 ka time slice, the $\delta^{18}O_w$ gradient was reversed compared to modern during this time. This gradient reversal likely reflects the same trends that were evident at 20 ka: an increase in the winter monsoon, and a decrease in the summer monsoon relative to today.

3.4. Time Slice: 8 ka

[26] Annually averaged insolation at 8 ka was similar to that at 15 ka (Figure 7). CO_2 and ice volume, however, were near their present-day values, thus significantly altering radiative forcing conditions relative to the 15 ka and 20 ka time slices [*Bard et al.*, 1996; *Petit et al.*, 1999, and references therein]. At 8 ka, perihelion, the point at which Earth is closest to the sun, occurred during August while today perihelion occurs during January. Thus, at 8 ka, Northern Hemisphere seasonality was enhanced relative to today and to the 15 ka and 20 ka time slices. In the absence of lowered CO_2 and greater ice volume as forcing factors, the importance of insolation was likely greater at 8 ka than at 15 ka and 20 ka.

3.4.1. SST

[27] At 8 ka, SSTs throughout the Arabian Sea were cooler than today by an average of 1.4° ± 1.3°C (Figure 10).

Table 4. Seawater Oxygen Isotope and Salinity Data From Joint Global Ocean Flux Study Cruises

Longitude	Latitude	Month	Depth, m	Salinity	$\delta^{18}O_w$
60.23	16.4	11	2.4	36.26	0.64
60.23	16.4	11	80	35.69	0.56
59.61	17.22	11	3	36.23	0.7
59.61	17.22	11	99	35.91	0.59
61.53	15.99	11	2	35.96	0.6
61.53	15.99	11	81	35.68	0.54
65.09	10.03	11	2	36.46	0.81
68.37	15.68	11	2	35.88	0.94
68.37	15.68	11	129	35.68	0.62
58.8	17.4	3	5	36.12	0.76
58.8	17.4	3	106	36.06	0.75
57.86	17.7	3	6	36	0.77
57.86	17.7	3	107	36.08	0.77
73.82	0.1	6	0	34.97	0.38
73.9	12.08	7	0	35.57	0.48
73.32	13.13	7	0	35.55	0.51
72.33	15	7	0	35.74	0.54
72.57	15.53	7	0	35.81	0.66
67.28	16.45	7	0	36.49	0.77
55.03	15	7	0	36.11	0.64
50.73	12.28	7	0	36.24	0.9
51.53	10.62	7	0	35.5	0.65
50.58	12.38	6	0	35.77	0.21
51.68	12.18	6	0	36.14	0.26
52.42	12.02	6	0	35.63	0.17
52.99	11.53	6	0	35.56	0.2
53.38	10.92	6	0	35.48	0.21
53.64	10.7	6	0	35.45	0.26
53.17	10.84	6	0	35.5	0.15
52.17	11.21	6	0	35.68	0.19
51.9	11.31	6	0	35.83	0.39
51.83	10.93	6	0	35.81	0.35
52.03	10.77	6	0	35.72	0.28
52.38	10.72	6	0	35.47	0.31
51.94	10.77	6	0	35.72	0.26
51.95	10.75	6	0	35.72	0.29
52.1	10.83	6	0	35.55	0.19
52.03	10.78	6	0	35.57	0.27
73.6	−4.3	6	0	35.45	0.49
73.8	0.1	6	0	34.97	0.38
76.4	2	6	0	34.74	0.32
79.5	3.9	6	0	34.97	0.39
78.7	6.4	7	0	35.65	0.42
76.5	7	7	0	35.72	0.56
75.7	8.6	7	0	35.5	0.46
74	12.1	7	0	35.57	0.48
73.3	13.1	7	0	35.55	0.51
72.3	15	7	0	35.74	0.54
72.6	15.5	7	0	35.81	0.66
67.3	16.5	7	0	36.49	0.77
55	15	7	0	36.11	0.64
45.1	11.8	7	0	36.42	0.8
48.2	11.5	7	0	36.08	0.8
49.6	11.7	7	0	36.08	0.8
50.7	12.3	7	0	36.24	0.9
51.5	10.6	7	0	35.5	0.65
46.4	2.3	7	0	34.96	0.55
41.1	3	8	0	34.71	0.35
40.2	−5.9	8	0	34.81	0.45
40.2	−7.2	8	0	34.81	0.45
51.15	14.17	8	0	35.89	0.31
51.26	15.08	8	0	35.71	0.23
51.27	15.05	8	0	35.69	0.24
51.3	14.49	8	0	35.71	0.27
51.27	14.53	8	0	35.68	0.25
51.29	14.55	8	0	35.72	0.32
51.34	14.38	8	0	35.72	0.24
51.36	14.41	8	0	35.75	0.21
51.37	14.31	8	0	35.72	0.17
51.38	14.31	8	0	35.74	0.29
51.54	14.43	8	0	35.74	0.2
52.39	15.33	8	0	35.71	0.18
53.1	16.1	8	0	35.75	0.27
52.46	16.02	8	0	35.69	0.21
52.23	16.1	8	0	35.69	0.15
52.3	16.09	8	0	35.67	0.24
52.39	16.06	8	0	35.68	0.23
52.46	16.05	8	0	35.67	0.23
52.42	16.04	8	0	35.68	0.25
52.53	15.58	8	0	35.69	0.27
52.45	16.03	8	0	35.7	0.23
53.01	15.54	8	0	35.9	0.32
53.01	15.53	8	0	35.99	0.14
52.58	15.4	8	0	36	0.12
52.48	14.45	8	0	35.71	0.17
52.4	13.57	8	0	35.97	0.32
52.31	13.16	8	0	36.2	0.36
52.23	12.46	8	0	35.86	0.32
51.4	12	8	0	36.28	0.3
51.44	11.4	8	0	35.36	0.15
52.11	11.38	8	0	35.64	0.19
52.4	11.44	8	0	35.67	0.22
53.34	10.42	8	0	35.51	0.18
51.5	10.27	8	0	35.66	0.33
51.46	10.01	8	0	35.75	0.35
51.5	9.58	8	0	35.63	0.36
52.52	6.6	8	0	35.65	0.33
53.01	6.23	8	0	35.52	0.22
53.1	5.3	8	0	35.46	0.3
53.28	4.19	8	0	35.34	0.28
53.38	3.03	8	0	35.38	0.23
53.43	2.06	8	0	35.37	0.2
53.45	1.44	8	0	35.39	0.26
53.38	1.53	8	0	35.37	0.39
53.43	1.46	8	0	35.38	0.33
53.43	1.42	8	0	35.36	0.25
53.58	0.59	8	0	35.52	0.26
54.13	0.17	8	0	35.49	0.3
54.3	−0.23	8	0	35.47	0.26
50.55	12.37	2	0	36.15	0.41
51.65	12.04	2	0	36.14	0.35
51.58	10.78	2	0	35.99	0.41
51.8	10.81	2	0	35.95	0.31
51.93	10.77	2	0	35.79	0.26
51.94	10.79	2	0	35.69	0.29
52.02	10.83	2	0	35.74	0.45
52.31	10.81	2	0	35.71	0.35
52.91	10.78	2	0	36.14	0.42
52.7	10.96	2	0	36.17	0.48
52.35	11.66	2	0	36.23	0.47
53.89	11.01	2	0	36.22	0.45
53.56	10.71	2	0	36.22	0.41
53.56	10.75	2	0	36.25	0.41
53.32	10.51	2	0	36.2	0.36
52.67	10.42	2	0	35.91	0.43
51.73	10.72	2	0	35.59	0.24
51.84	10.78	2	0	35.85	0.39
52.62	10.93	2	0	35.58	0.25
52.84	11.97	2	0	36.17	0.32
53.42	14.16	2	0	36.2	0.41
52.89	15.87	2	0	36.22	0.43
52.84	15.96	2	0	36.22	0.52
52.69	16.05	2	0	36.12	0.42
52.61	16.07	2	0	36.2	0.26
52.54	16.17	2	0	36.22	0.42
51.83	14.55	2	0	36.19	0.36
51.76	14.47	2	0	36.05	0.35
51.52	14.8	2	0	36.2	0.29
51.41	15.13	2	0	36.17	0.37
51.87	14.78	2	0	36.18	0.4

Table 4. (continued)

Longitude	Latitude	Month	Depth, m	Salinity	$\delta^{18}O_w$
52.85	14.03	2	0	36.15	0.37
53.24	13.71	2	0	36.17	0.46
54.64	−1.15	2	0	35.22	0.23
54.54	−1.09	2	0	35.2	0.25
54.23	−0.16	2	0	35.32	0.11
53.85	0.93	2	0	35.35	0.22
53.58	1.91	2	0	35.39	0.31
53.46	2.29	2	0	35.38	0.18
53.76	3.35	2	0	35.4	0.24
52.77	4.2	2	0	35.55	0.28
52.75	4.48	2	0	35.66	0.24
52.47	6.19	2	0	35.73	0.28
52.46	6.31	2	0	35.7	0.3
52.42	6.39	2	0	35.71	0.23
52.47	6.15	2	0	35.75	0.26
52.35	6.09	2	0	35.75	0.28
52.18	6.02	2	0	35.78	0.22
51.42	6.65	2	0	35.83	0.26
50.67	7.33	2	0	35.93	0.25
50.52	7.63	2	0	35.91	0.35
50.64	7.92	2	0	35.84	0.27
51.07	7.31	2	0	35.82	0.29
51.32	7.54	2	0	35.76	0.17
51.91	9.02	2	0	35.81	0.22
52.5	9.52	2	0	36.12	0.27
52	10.9	2	0	36.15	0.2
52.04	11.19	2	0	36.1	0.26
52.07	11.29	2	0	36.1	0.26
52.02	11.29	2	0	36.09	0.18
52.01	11.72	2	0	36.11	0.29
51.8	12.11	2	0	36.11	0.31
52.22	12.02	2	0	35.98	0.15
53.36	12.01	2	0	36.03	0.29
53.86	12.09	2	0	36.04	0.36
54.75	12	2	0	36.28	0.23
55.05	12.21	2	0	36.25	0.26
54.98	12.17	2	0	36.22	0.27
55.04	12.12	2	0	36.33	0.44
53.91	12.02	2	0	36.05	0.39
52.44	12.86	2	0	36.08	0.3
51.55	12.84	2	0	36.07	0.26
50.09	12.77	2	0	36.22	0.31
50.16	13.18	2	0	36.09	0.31
50.26	13.53	2	0	36.04	0.39

Thus, from 15 ka to 8 ka, the Arabian Sea experienced a 1.5°C warming associated with the deglaciation. Sites in the eastern Arabian Sea exhibit larger cold anomalies than those in the western Arabian Sea, resulting in a decrease in the strength of the SST gradient across the basin.

[28] Our finding that SSTs throughout the basin were cooler than present at 8 ka is corroborated by two Arabian Sea sites with Holocene alkenone-SST records that demonstrate that SSTs were cooler at 7 ka than they are today [*Kim et al.*, 2004]. While the Arabian Sea warmed from the early Holocene to today, sites throughout the subtropical North Atlantic and Mediterranean regions cooled [*Marchal et al.*, 2002; *Kim et al.*, 2004, and references therein]. This cooling trend is commonly attributed to decreasing solar insolation. In the Arabian Sea region, however, modeling studies indicate that the enhanced seasonality during this time would result in an increase in both the summer and winter monsoons [*Kutzbach and Gallimore*, 1988; *Prell and Kutzbach*, 1992; *Liu et al.*, 2003]. The colder SSTs during this time is therefore likely the result of stronger than present summer monsoon upwelling in the western Arabian Sea and winter monsoon mixing in the northeastern Arabian Sea. A number of studies, most of which utilize the percentage of the planktonic foraminifer *Globigerina bulloides* as a monsoon upwelling indicator, have indicated that this time period was one of greater summer monsoon strength [*Prell*, 1984; *Sirocko et al.*, 1993; *Naidu and Malmgren*, 1995; *Overpeck et al.*, 1996; *Fleitmann et al.*, 2003; *Gupta et al.*, 2003]. Given the negative SST anomalies we observe outside of the summer monsoon upwelling region, however, our data suggest that an increase in summer monsoon intensity must have been accompanied by an increase in winter monsoon intensity. Thus, while the basin-wide cold anomalies observed in the 20 and 15 ka time slices were likely due, in large part, to the influence of glacial boundary conditions, the basin-wide cold anomalies in the 8 ka time slice resulted from greater seasonality and strengthened winter and summer monsoons associated with solar insolation conditions.

3.4.2. The $\delta^{18}O_w$

[29] Throughout the basin $\delta^{18}O_w$ was, on average, 0.5‰ lower at 8 ka than it is today (Figure 10). The low anomalies are larger in the eastern Arabian Sea than in the western Arabian Sea, thereby reducing the cross basinal gradient that is observed today. Increased transport of subsurface waters to the surface during both monsoon seasons could account for the overall decrease in $\delta^{18}O_w$. In this case, the decreased gradient would require that the increase in winter monsoon mixing was greater than the increase in summer monsoon upwelling. Alternatively, increased precipitation and runoff associated with a strengthened summer monsoon contributed to the $\delta^{18}O_w$ decrease. Sites in the eastern Arabian Sea would be more affected by increased runoff than sites in the west given the distribution of rainfall and rivers in the region, consistent with our results.

4. Summary and Conclusions

[30] We have constructed Arabian Sea SST and $\delta^{18}O_w$ maps for four time periods in order to gain an understanding of the history of the Indian Monsoon. The occurrence of basin-wide SST changes in the 8 ka, 15 ka, and 20 ka time slices suggests that long-term variations in the SST pattern in this region are a function not just of monsoon-induced upwelling, but of other factors as well. Consistent with modeling studies, we find that glacial boundary conditions have a profound influence on Arabian Sea SST that is irrespective of monsoon upwelling [*Broccoli*, 2000]. Lowered CO_2 and increased ice volume contributed to basin-wide cold anomalies relative to today in the Arabian Sea at 15 ka and 20 ka via direct radiative forcing. Superimposed upon the cold anomalies are changes in the SST pattern that imply an increase (decrease) in winter (summer) monsoon strength relative to today. Absolute SSTs, as well as the SST pattern, at the 8 ka time slice reflect the relaxation of glacial boundary conditions and enhanced Northern Hemisphere seasonality, which resulted in stronger summer and winter monsoons relative to today. While several previous studies have inferred a stronger than present summer monsoon during the early Holocene,

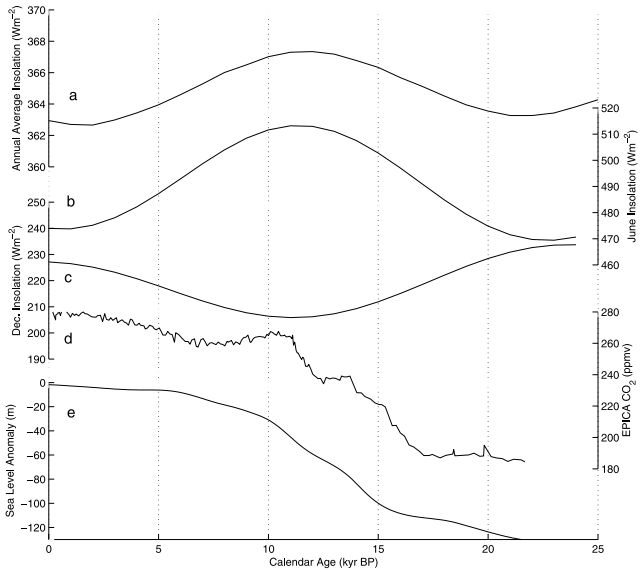

Figure 7. Insolation at 30°N for (a) annual average, (b) June, and (c) December [*Berger*, 1978; *Berger and Loutre*, 1991]. (d) Atmospheric CO_2 in the European Programme for Ice Coring in Antarctica (EPICA) Dome C ice core [*Monnin et al.*, 2001]. (e) Sea level as determined from Barbados corals [*Fairbanks*, 1989; *Bard et al.*, 1990].

the enhanced winter monsoon has, to our knowledge, only been inferred from modeling studies [e.g., *Overpeck et al.*, 1996; *Liu et al.*, 2003]. The $\delta^{18}O_w$ patterns for these time slices are consistent with our interpretation of the SST analyses. Additionally, we interpret the <1‰ increases in $\delta^{18}O_w$ during the 15 ka and 20 ka time slices as reflecting weaker than present evaporation, possibly in concert with changes in the strength of both the summer and winter monsoons. Lower than present $\delta^{18}O_w$ in the 8 ka time slice may be due to increased precipitation and/or runoff into the Arabian Sea along with changes in upper oceanic dynamics.

[31] Mg/Ca-derived SSTs at the LGM suggest lower SSTs than originally reconstructed by the CLIMAP study [*CLIMAP Project Members*, 1981]. These results add to a growing body of evidence of alkenone and foraminiferal abundance derived SST estimates implying that SSTs in the Arabian Sea were 2°–4°C cooler than present at the LGM [*Emeis et al.*, 1995; *Bard et al.*, 1997; *Rostek et al.*, 1997; *Sonzogni et al.*, 1998; *Cayre and Bard*, 1999; *Higginson et al.*, 2004; *Naidu and Malmgren*, 2005].

[32] Our interpretations of temperature and $\delta^{18}O_w$ variations presume that there were no large changes in the temperature or $\delta^{18}O_w$ of Arabian Sea source waters over the past 20,000 years. Waters upwelled in the Arabian Sea originate in the subtropical Indian Ocean and are markedly colder and fresher than the surface waters of the Arabian

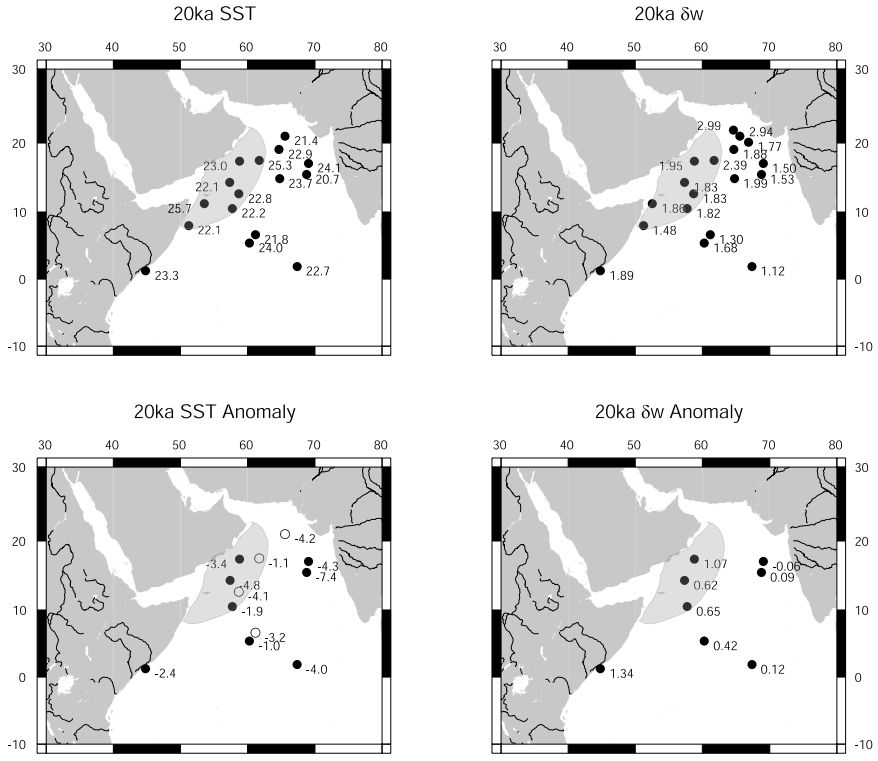

Figure 8. Surface conditions at 20 ka: (top) Mg/Ca sea surface temperature and $\delta^{18}O_w$ and (bottom) SST and $\delta^{18}O_w$ anomalies relative to the 0 ka time slice. Solid circles represent cores for which a "modern" (core top) and a time slice sample were available. Open circles represent cores for which anomalies were calculated using the time slice sample and the nearest modern core top sample. Shading is as for Figure 2.

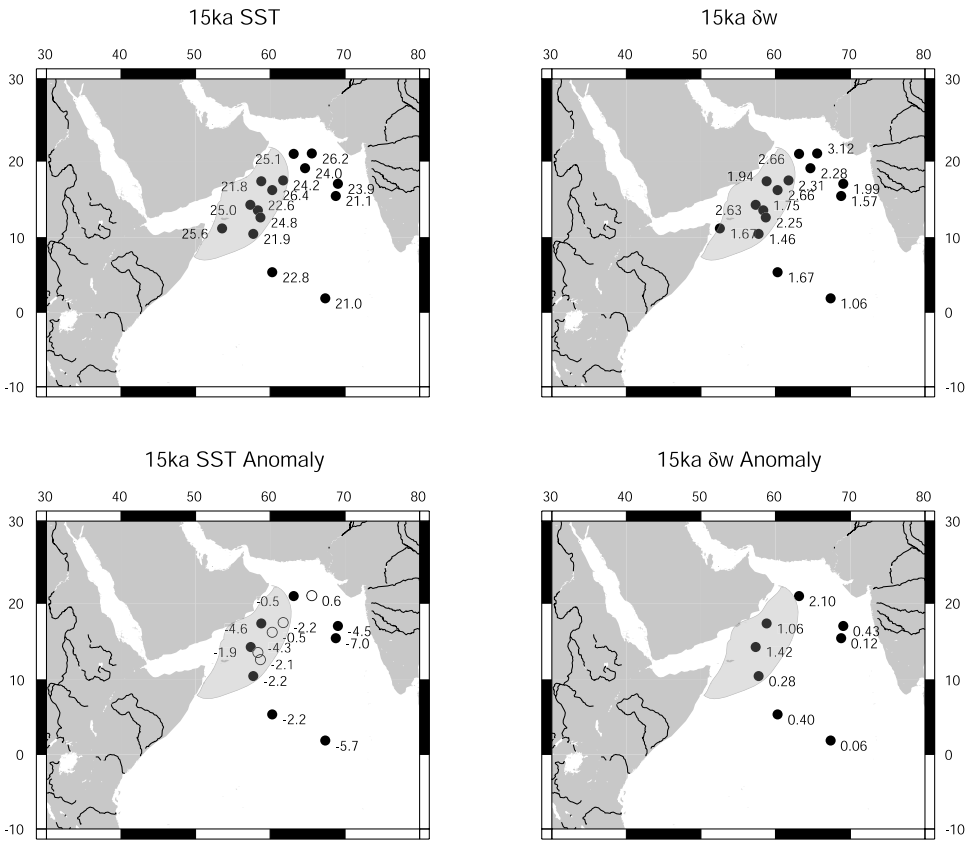

Figure 9. Surface conditions at 15 ka: (top) Mg/Ca SST and $\delta^{18}O_w$ and (bottom) SST and $\delta^{18}O_w$ anomalies relative to the 0 ka time slice. Symbols are as for Figure 8; shading is as for Figure 2.

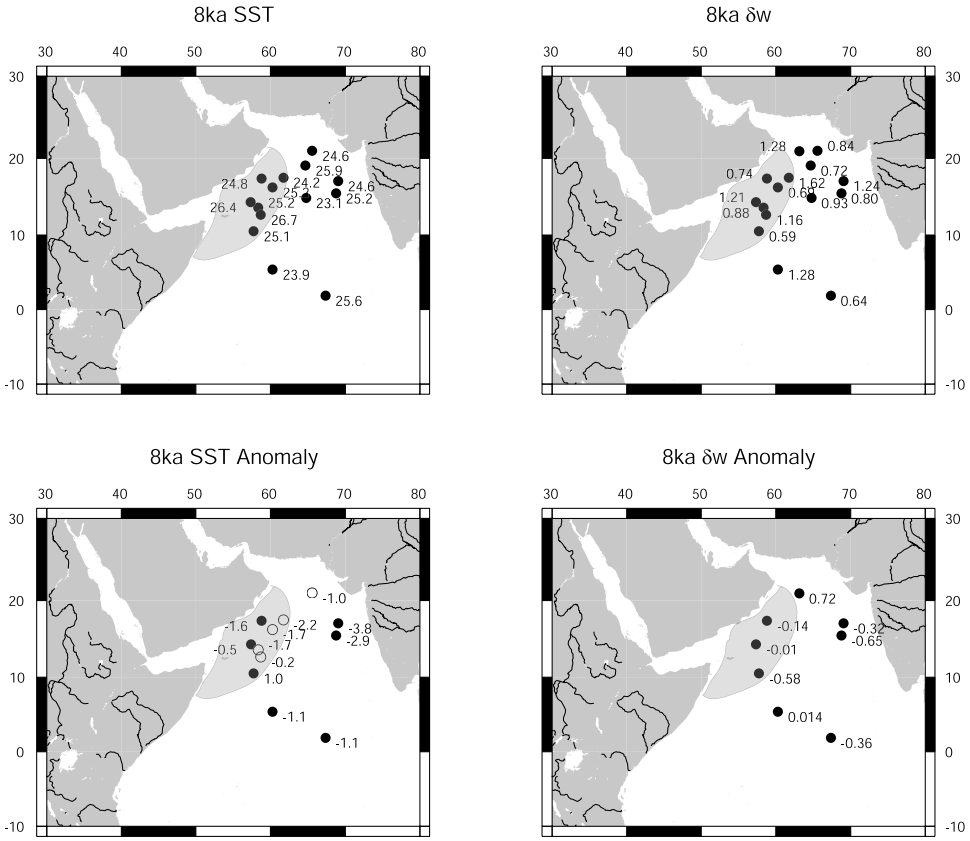

Figure 10. Surface conditions at 8 ka: (top) Mg/Ca SST and $\delta^{18}O_w$ and (bottom) SST and $\delta^{18}O_w$ anomalies relative to the 0 ka time slice. Symbols are as for Figure 8; shading is as for Figure 2.

Sea [*Schott et al.*, 2002]. Changes in the properties and/or the flux of these source waters could affect the surface properties of the Arabian Sea, particularly within upwelling regions.

[33] The primary radiative forcing factors (CO_2, ice volume, and solar insolation) appear to exert differing degrees of influence on Arabian Sea climate over the past 20ka. Sea surface conditions at 15 ka and 20 ka in the Arabian Sea were very similar, despite very different solar insolation conditions. Conversely, conditions recorded by the 8 ka and 15 ka time slices are very different, despite similar insolation conditions during the two time periods. This suggests that, during glacial periods, lowered CO_2 and increased ice volume are the dominant radiative forcing factors for this region. During interglacial periods, however, solar insolation dominates the radiative forcing.

[34] **Acknowledgments.** We would like to thank Rose Came, Simon Thorrold, and Scot Birdwhistell for laboratory assistance and technical support with the ICP-MS as well as Rindy Ostermann for technical support with the carbonate mass spectrometer. We also thank Yair Rosenthal and Suzanne Perron-Cashman for analyses of the 0 ka samples. Frank Sirocko, Andreas Lückge, and Bill Curry kindly provided samples. Bill Curry also provided the $\delta^{18}O_w$ measurements from the JGOFS TN-41 and TN-47 cruises (funded by National Science Foundation grant OCE93-11199). Analyses were funded by a SGER grant from the NSF (OCE03-34598). Funding was also provided by a Schlanger Ocean Drilling Program Fellowship (to K.A.D.) and NSF grant OCE02-20776 (to D.W.O.).

References

Anand, P., H. Elderfield, and M. H. Conte (2003), Calibration of Mg/Ca thermometry in planktonic foraminifera from a sediment trap time series, *Paleoceanography*, *18*(2), 1050, doi:10.1029/2002PA000846.

Anderson, D. M., J. T. Overpeck, and A. K. Gupta (2002), Increase in the Asian southwest monsoon during the past four centuries, *Science*, *297*, 596–599.

Bard, E., B. Hamelin, and R. G. Fairbanks (1990), U-Th ages obtained by mass spectrometry in corals from Barbados: Sea level during the past 130,000 years, *Nature*, *346*, 456–458.

Bard, E., B. Hamelin, M. Arnold, L. Montaggioni, G. Cabioch, G. Faure, and F. Rougerie (1996), Deglacial sea-level record from Tahini corals and the timing of global meltwater discharge, *Nature*, *382*, 241–244.

Bard, E., F. Rostek, and C. Sonzogni (1997), Interhemispheric synchrony of the last deglaciation inferred from alkenone palaeothermometry, *Nature*, *385*, 707–710.

Bard, E., F. Rostek, J.-L. Turon, and S. Gendreau (2000), Hydrological impact of Heinrich events in the subtropical North Atlantic, *Science*, *289*, 1321–1324.

Berger, A., and M. F. Loutre (1991), Insolation values for the climate of the last 10 million years, *Quat. Sci. Rev.*, *10*, 297–317.

Berger, A. L. (1978), Long-term variations of caloric insolation resulting from the Earth's orbital variations, *Quat. Res.*, *9*, 139–167.

Bice, K. L., G. D. Layne, and K. A. Dahl (2005), Application of secondary ion mass spectrometry to the determination of Mg/Ca in rare, delicate, or altered planktonic foraminifera: Examples from the Holocene, Paleogene, and Cretaceous, *Geochem. Geophys. Geosyst.*, *6*, Q12P07, doi:10.1029/2005GC000974.

Boyle, E. A., and L. D. Keigwin (1985), Comparison of Atlantic and Pacific paleochemical records for the last 250,000 years: Changes in deep ocean circulation and chemical inventories, *Earth Planet. Sci. Lett.*, *76*, 135–150.

Boyle, E. A., and Y. Rosenthal (1996), Chemical hydrography of the South Atlantic during the last glacial maximum: $\delta^{13}C$ versus Cd, in *The South Atlantic: Present and Past Circulation*, edited by G. Wefer et al., pp. 423–443, Springer, New York.

Broccoli, A. J. (2000), Tropical cooling at the Last Glacial Maximum: An atmosphere-mixed layer ocean model simulation, *J. Clim.*, *13*, 951–976.

Cayre, O., and E. Bard (1999), Planktonic foraminiferal and alkenone records of the last deglaciation from the eastern Arabian Sea, *Quat. Res.*, *52*, 337–342.

Clemens, S., W. Prell, D. Murray, G. Shimmield, and G. Weedon (1991), Forcing mechanisms of the Indian Ocean monsoon, *Nature*, *353*, 720–725.

Clemens, S. C., and W. L. Prell (2003), A 350,000 year summer-monsoon multi-proxy stack from the Owen Ridge, northern Arabian Sea, *Mar. Geol.*, *201*, 35–51.

CLIMAP Project Members (1981), Seasonal reconstruction of the Earth's surface at the Last Glacial Maximum, *Geol. Soc. Am. Map Chart Ser.*, *MC-36*.

Conan, S. M.-H., and G.-J. A. Brummer (2000), Fluxes of planktic foraminifera in response to monsoonal upwelling on the Somalia Basin margin, *Deep Sea Res., Part II*, *47*, 2207–2227.

Curry, W. B., D. R. Ostermann, M. V. S. Guptha, and V. Ittekkot (1992), Foraminiferal production and monsoonal upwelling in the Arabian Sea: Evidence from sediment traps, in *Upwelling Systems: Evolution Since the Early Miocene*, edited by C. P. Summerhayes, W. L. Prell, and K. C. Emeis, *Geol. Soc. Spec. Publ. London*, *64*, 93–106.

Delaygue, G., E. Bard, C. Rollion, J. Jouzel, M. Stievenard, J.-C. Duplessy, and G. Ganssen (2001), Oxygen isotope/salinity relationship in the northern Indian Ocean, *J. Geophys. Res.*, *106*, 4565–4574.

Emeis, K.-C., D. M. Anderson, H. Doose, D. Kroon, and D. Schulz-Bull (1995), Sea-surface temperatures and the history of monsoon upwelling in the Northwest Arabian Sea during the last 500,000 years, *Quat. Res.*, *43*, 355–361.

Fairbanks, R. G. (1989), A 17,000-year glacio-eustatic sea level record: Influence of glacial melting rates on the younger dryas event and deep-ocean circulation, *Nature*, *342*, 637–642.

Fleitmann, D., S. J. Burns, M. Mudelsee, U. Neff, J. Kramers, A. Mangini, and A. Matter (2003), Holocene forcing of the Indian Monsoon recorded in a stalagmite from southern Oman, *Science*, *300*, 1737–1739.

Fontugne, M. R., and J. C. Duplessy (1986), Variations of the monsoon regime during the upper Quaternary: Evidence from the carbon isotopic record of organic matter in north Indian Ocean sediments, *Palaeogeogr. Palaeoclimatol. Palaeoecol.*, *56*, 69–88.

Gupta, A. K., D. M. Anderson, and J. T. Overpeck (2003), Abrupt changes in the Asian southwest monsoon during the Holocene and their links to the North Atlantic Ocean, *Nature*, *421*, 354–357.

Higginson, M. J., M. A. Altabet, L. Wincze, T. D. Herbert, and D. W. Murray (2004), A solar (irradiance) trigger for millennial-scale abrupt changes in the southwest monsoon?, *Paleoceanography*, *19*, PA3015, doi:10.1029/2004PA001031.

Kim, J.-H., N. Rimbu, S. J. Lorenz, G. Lohmann, S.-I. Nam, S. Schouten, C. Rühlemann, and R. R. Schneider (2004), North Pacific and North Atlantic sea-surface temperature variability during the Holocene, *Quat. Sci. Rev.*, *23*, 2141–2154.

Kodera, K. (2004), Solar influence on the Indian Ocean Monsoon through dynamical processes, *Geophys. Res. Lett.*, *31*, L24209, doi:10.1029/2004GL020928.

Kutzbach, J. E., and R. G. Gallimore (1988), Sensitivity of a coupled atmosphere/mixed layer ocean model to changes in orbital forcing at 9000 years B.P., *J. Geophys. Res.*, *93*, 803–821.

Kutzbach, J. E., P. J. Guetter, P. J. Behling, and R. Selin (1993), Simulated climate changes: Results of the COHMAP climate-model experiments, in *Global Climates Since the Last Glacial Maximum*, edited by H. E. Wright Jr. et al., pp. 24–93, Univ. of Minn. Press, Minneapolis.

Lea, D. W., D. K. Pak, L. C. Peterson, and K. A. Hughen (2003), Synchroneity of tropical and high-latitude Atlantic temperatures over the last glacial termination, *Science*, *301*, 1361–1364.

Levitus, S., and T. Boyer (1994), *World Ocean Atlas 1994*, vol. 4, *Temperature, NOAA Atlas NESDIS*, vol. 13, NOAA, Silver Spring, Md.

Liu, Z., B. Otto-Bleisner, J. Kutzback, L. Li, and C. Shields (2003), Coupled climate simulation of the evolution of global monsoons in the Holocene, *J. Clim.*, *16*, 2472–2490.

Locke, S., and R. C. Thunell (1988), Paleoceanographic record of the last glacial/interglacial cycle in the Red Sea and Gulf of Aden, *Palaeogeogr. Palaeoclimatol. Palaeoecol.*, *64*, 163–187.

Marchal, O., et al. (2002), Apparent long-term cooling of the sea surface in the northeast Atlantic and Mediterranean during the Holocene, *Quat. Sci. Rev.*, *21*, 455–483.

Mix, A. C., E. Bard, and R. Schneider (2001), Environmental processes of the Ice Age: Land, ocean, glaciers (EPILOG), *Quat. Sci. Rev.*, *20*, 627–657.

Monnin, E., A. Indermühle, A. Dällenbach, J. Flückiger, B. Stauffer, T. F. Stocker, D. Raynaud, and J.-M. Barnola (2001), Atmospheric CO_2 concentrations over the last glacial termination, *Science*, *291*, 112–114.

Mulitza, S., D. Bolotovskoy, B. Donner, H. Meggers, A. Paul, and G. Wefer (2003), Temperature: $\delta^{18}O$ relationships of planktonic foraminifera collected from surface waters, *Palaeogeogr. Palaeoclimatol. Palaeoecol.*, *202*, 143–152.

Naidu, P. D., and B. A. Malmgren (1995), A 2,200 year periodicity in the Asian monsoon system, *Geophys. Res. Lett.*, *22*, 2361–2364.

Naidu, P. D., and B. A. Malmgren (2005), Seasonal sea surface temperature contrast between the Holocene and last glacial period in the western Arabian Sea (Ocean Drilling Project Site 723A): Modulated by monsoon upwelling, *Paleoceanography*, *20*, PA1004, doi:10.1029/2004PA001078.

Naqvi, W. A., and R. G. Fairbanks (1996), A 27,000 year record of Red Sea outflow: Implication for timing of post-glacial monsoon intensification, *Geophys. Res. Lett.*, *23*, 1501–1504.

Oberhuber, J. M. (1988), An atlas based on the COADS data set: The budget of heat, buoyancy and turbulent kinetic energy at the surface of the global ocean, *Tech. Rep. 15*, Max-Planck-Inst. für Meteorol., Hamburg, Germany.

Overpeck, J. T., D. M. Anderson, S. Trumbore, and W. L. Prell (1996), The Southwest Monsoon over the last 18,000 years, *Clim. Dyn.*, *12*, 213–225.

Peeters, F. J. C., G. A. Brummer, and G. Ganssen (2002), The effect of upwelling on the distribution and stable isotope composition of *Globigerina bulloides* and *Globigerinoides ruber* (planktic foraminifera) in modern surface waters of the NW Arabian Sea, *Global Planet. Change*, *34*, 269–291.

Petit, J. R., et al. (1999), Climate and atmospheric history of the past 420,000 years from the Vostok ice core, Antarctica, *Nature*, *399*, 429–436.

Pinot, S., G. Ramstein, S. P. Harrison, I. C. Prentice, J. Guiot, M. Stute, and S. Joussame (1999), Tropical paleoclimates of the Last Glacial Maximum: Comparison of Paleoclimate Modeling Intercomparison Project (PMIP) simulations and paleodata, *Clim. Dyn.*, *15*, 857–874.

Prell, W. L. (1984), Variation of monsoonal upwelling: A response to changing solar radiation, in *Climate Processes and Climate Sensitivity*, *Geophys. Monogr. Ser.*, vol. 29, edited by J. Hansen and T. Takahashi, pp. 48–57, AGU, Washington, D. C.

Prell, W. L., and J. E. Kutzbach (1992), Sensitivity of the Indian monsoon to forcing parameters and implications for its evolution, *Nature*, *360*, 647–651.

Reichart, G. J., L. J. Lourens, and W. J. Zachariasse (1998), Temporal variability in the northern Arabian Sea oxygen minimum zone (OMZ) during the last 225,000 years, *Paleoceanography*, *13*, 607–621.

Rosenthal, Y., and G. P. Lohmann (2002), Accurate estimation of sea surface temperatures using dissolution-corrected calibrations for Mg/Ca paleothermometry, *Paleoceanography*, *17*(3), 1044, doi:10.1029/2001PA000749.

Rosenthal, Y., E. A. Boyle, L. Labeyrie, and D. Oppo (1995), Glacial enrichments of authigenic Cd and U in Subantarctic sediments: A climatic control on the elements' oceanic budget?, *Paleoceanography*, *10*, 395–413.

Rostek, F., G. Ruhland, F. C. Bassinot, P. J. Müller, L. D. Labeyrie, Y. Lancelot, and E. Bard (1993), Reconstructing sea surface temperature and salinity using $\delta^{18}O$ and alkenone records, *Nature*, *364*, 319–321.

Rostek, F., E. Bard, L. Beaufort, C. Sonzogni, and G. Ganssen (1997), Sea surface temperature and productivity records for the past 240 kyr in the Arabian Sea, *Deep Sea Res., Part II*, *44*, 1461–1480.

Schmidt, M. W., H. J. Spero, and D. W. Lea (2004), Links between salinity variation in the Caribbean and North Atlantic thermohaline circulation, *Nature*, *428*, 160–163.

Schott, F. A., M. Dengler, and R. Schoenefeldt (2002), The shallow overturning circulation of

the Indian Ocean, *Prog. Oceanogr.*, *53*, 57–103.

Schrag, D. P., J. F. Adkins, K. McIntyre, J. L. Alexander, D. A. Hodell, C. D. Charles, and J. F. McManus (2002), The oxygen isotopic composition of seawater during the Last Glacial Maximum, *Quat. Sci. Rev.*, *21*, 331–342.

Sirocko, F. (1989), Zur akkumulation von Staubsedimenen im nördlichen Indischen Ozean: Anzeiger der Klimagerschichte Arabiens und Indiens, Ph.D. thesis, Geol.-Paläontol. Inst., Univ. zu Kiel, Kiel, Germany.

Sirocko, F., and H. Lange (1991), Clay-mineral accumulation rates in the Arabian Sea during the late Quaternary, *Mar. Geol.*, *97*, 105–119.

Sirocko, F., and M. Sarnthein (1989), Windborne deposits in the Northwestern Indian Ocean: Record of Holocene sediments versus satellite data, in *Paleoclimatology and Paleometeorology: Modern and Past Patterns of Global Atmospheric Transport*, edited by M. Leinin and M. Sarnthein, *NATO ASI Ser., Ser. C*, vol. 282, pp. 401–433, Springer, New York.

Sirocko, F., M. Sarnthein, H. Lange, and H. Erlenkeuser (1991), Atmospheric summer circulation and coastal upwelling in the Arabian Sea during the Holocene and last glaciation, *Quat. Res.*, *36*, 72–93.

Sirocko, F., M. Sarnthein, H. Erlenkeuser, H. Lange, M. Arnold, and J. C. Duplessy (1993), Century-scale events in monsoonal climate over the past 24,000 years, *Nature*, *364*, 322–324.

Sirocko, F., D. Garbe-Schönberg, and C. Devey (2000), Processes controlling trace element geochemistry of Arabian Sea sediments during the last 25,000 years, *Global Planet. Change*, *26*, 217–303.

Sonzogni, C., E. Bard, and F. Rostek (1998), Tropical sea-surface temperatures during the last glacial period: A view based on alkenones in Indian Ocean sediments, *Quat. Sci. Rev.*, *17*, 1185–1201.

Stuiver, M., and P. J. Reimer (1993), Extended C-14 data-base and revised Calib 3.0 C-14 age calibration program, *Radiocarbon*, *35*, 215–230.

Waelbroeck, C., L. Labeyrie, J. C. Duplessy, J. Guiot, M. Labracherie, H. Leclaire, and J. Duprat (1998), Improving past sea surface temperature estimates based on planktonic fossil faunas, *Paleoceanography*, *13*, 272–283.

K. A. Dahl, Scripps Institution of Oceanography, 9500 Gilman Drive, Department 0244, La Jolla, CA 92093, USA. (kadahl@ucsd.edu)

D. W. Oppo, Department of Geology and Geophysics, Woods Hole Oceanographic Institution, Woods Hole, MA 02543, USA.